Supplementary Materials for

The Ccr4-Not complex monitors the translating ribosome for codon optimality

Robert Buschauer*, Yoshitaka Matsuo*, Takato Sugiyama, Ying-Hsin Chen, Najwa Alhusaini, Thomas Sweet, Ken Ikeuchi, Jingdong Cheng, Yasuko Matsuki, Risa Nobuta, Andrea Gilmozzi, Otto Berninghausen, Petr Tesina, Thomas Becker, Jeff Coller†, Toshifumi Inada†, Roland Beckmann†

*These authors contributed equally to this work.
†Corresponding author. Email: beckmann@genzentrum.lmu.de (R.B.); toshifumi.inada.a3@tohoku.ac.jp (T.I.); jmc71@case.edu (J.C.)

Published 17 April 2020, *Science* **368**, eaay6912 (2020)
DOI: 10.1126/science.aay6912

This PDF file includes:

Other Supplementary Material for this manuscript includes the following:
(available at science.sciencemag.org/content/368/6488/eaay6912/suppl/DC1)

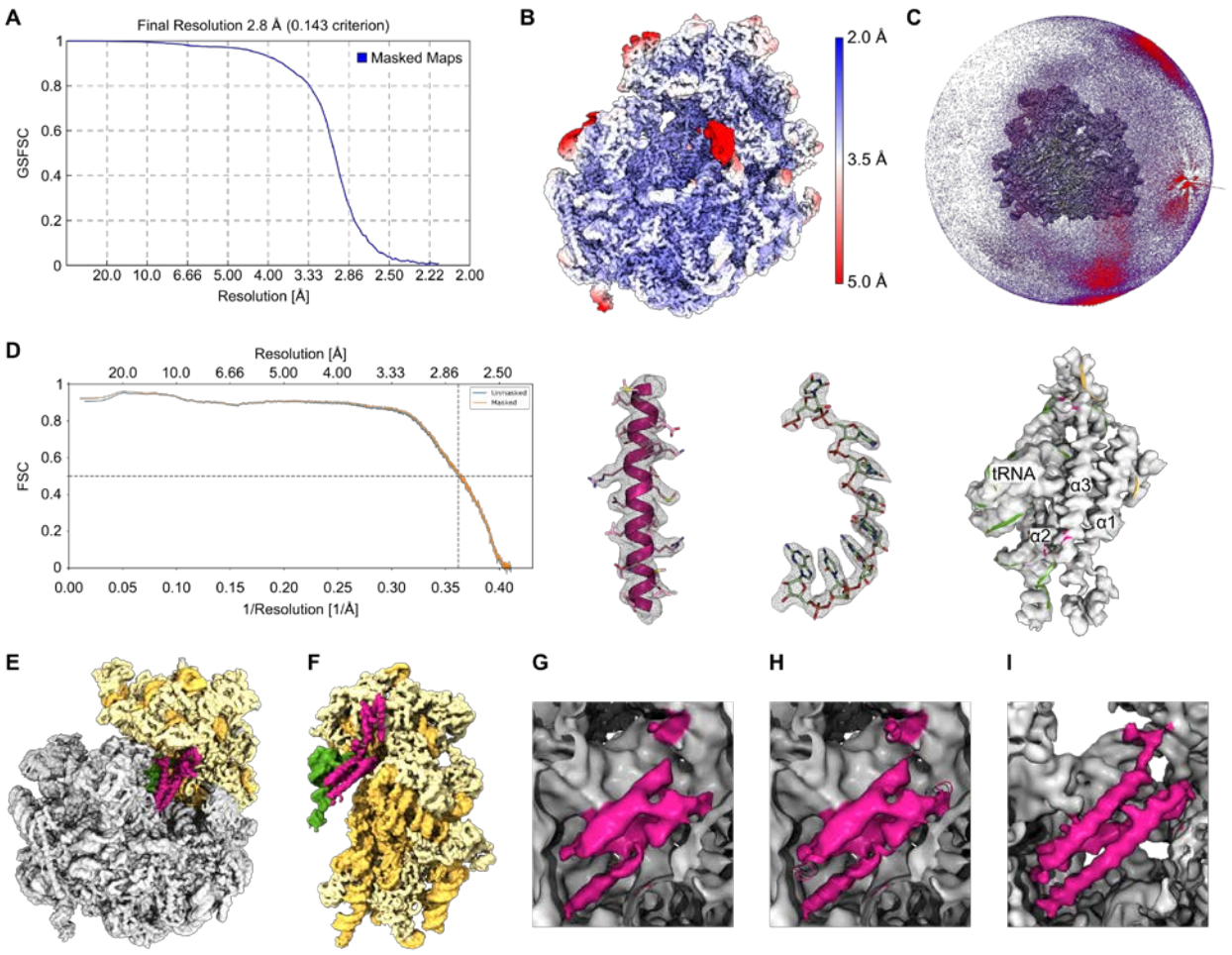

Fig. S1.

(**A**) Gold Standard Fourier shell correlation of the Not5 bound 80S ribosome. (**B**) Cryo-EM density of the Not5 bound 80S ribosome colored according to local resolution. (**C**) Euler angle distribution of the final Not5 bound 80S reconstruction. (**D**) Model-to-map-FSC of the Not5 bound 80S ribosome and representative densities of a helix of the Not5-NTD, of ribosomal RNA and the full Not5-NTD. (**E**) Cryo-EM density of the cross-linked Not5 bound 80S ribosome (**F**) Cryo-EM density of the 40S subunit, the P-site tRNA and the extended Not5-NTD of the cross-linked Not5 bound 80S ribosome. (**G**) Cryo-EM density of the Not5 bound 80S ribosome in absence of antibiotics. (**H**) Cryo-EM density of the Not5 bound 80S ribosome in absence of antibiotics with

a rigid body docked model of Not5-NTD. (**I**) Cryo-EM density of the Not5 bound 80S ribosome stabilized by tigecycline..

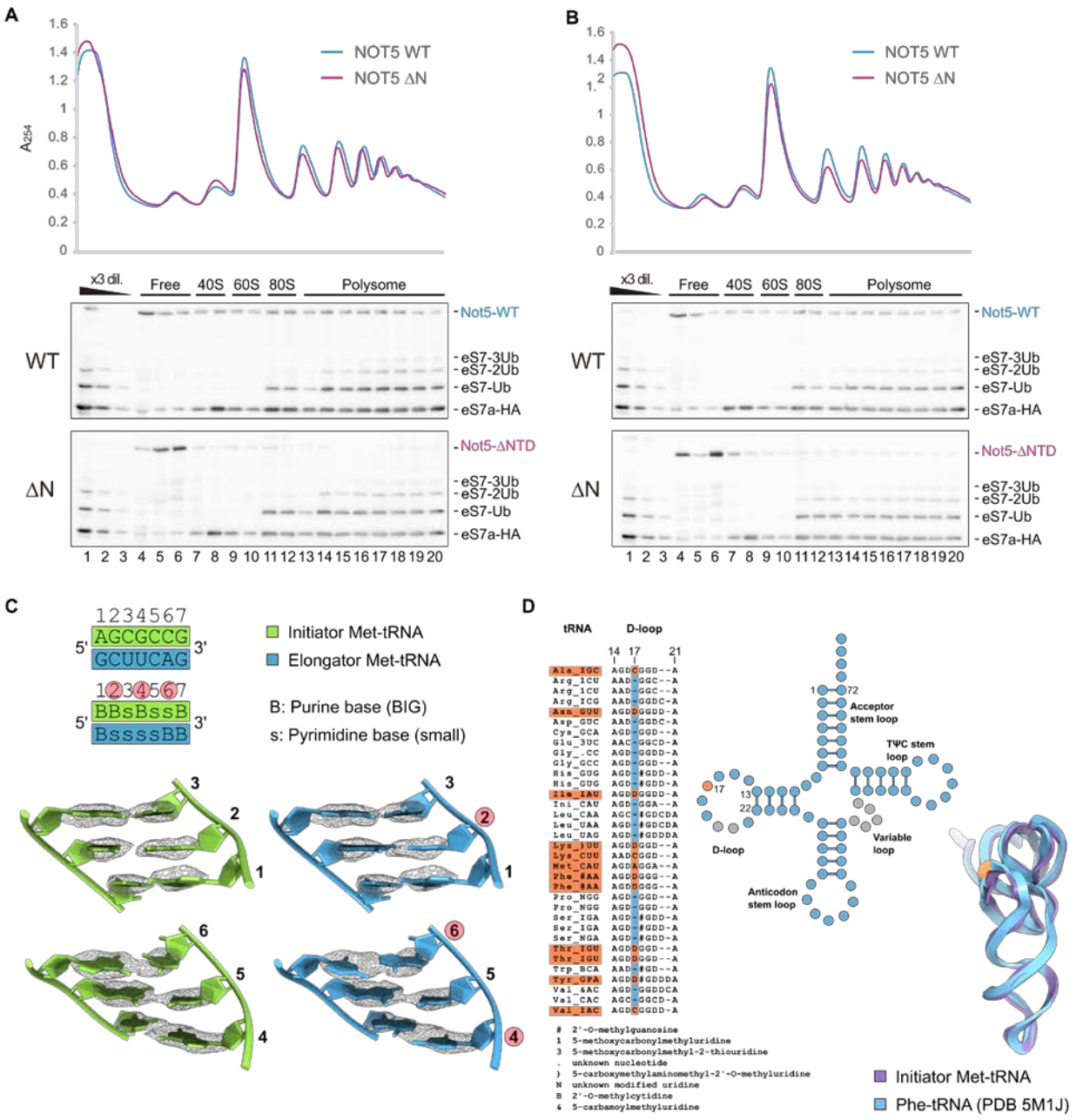

Fig. S2.

(**A** to **B**). Replicates of density gradient fractionation profiles of Not5-HA and Not5-ΔNTD-HA strains and corresponding Western blot detection of the respective Not5 proteins and of ribosomal protein eS7-HA. The signals at higher molecular weight correspond to ubiquitinated species of eS7-HA. (**C**) Comparison between initiator and elongator Met-tRNA. The elongator tRNA does not fit into the cryo-EM density (grey mesh, compare positions 2, 4, 6). (**D**) Comparison of tRNAs

featuring short and long D-loops as defined by absence or presence of a nucleotide in position 17 (List according to *http://trna.bioinf.uni-leipzig.de/*).

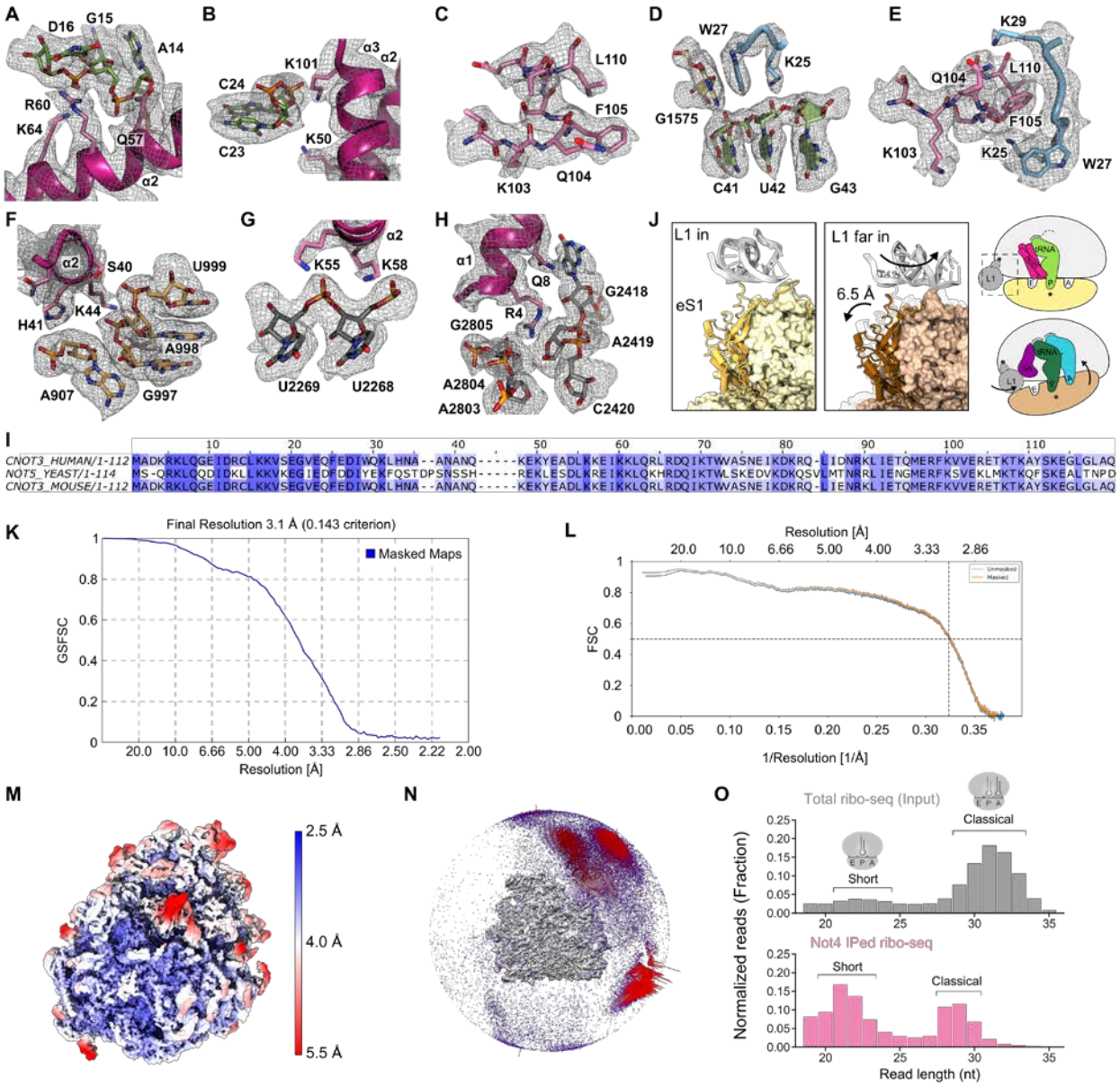

Fig. S3.

(**A**) Interactions of Not5-NTD with the D-loop of $tRNA_i^{Met}$. (**B**) Interactions of Not5 with the D-stem of $tRNA_i^{Met}$. (**C** to **E**) Interactions between the tRNA-clamp-motif (tCM) of Not5, the anticodon stem loop of $tRNA_i^{Met}$, the N-terminus of eS25 and 18S rRNA. (**F**) Interactions of Not5-NTD with 18S rRNA. (**G** to **H**) Interactions of Not5 with 25S rRNA. (**I**) Sequence alignment of the Not5-NTD from human, yeast and mouse (aligned with T-Coffee, *https://www.ebi.ac.uk/Tools/msa/tcoffee/*). (**J**) Movement of the L1 stalk base from the in-position

in the non-rolled (--/PP/--) ribosome to the far-in position in the eIF5A bound rolled (AA/PP/--) ribosome. (**K**) Gold Standard Fourier shell correlation of the eIF5A bound 80S ribosome. (**L**) Model-to-map-FSC of the eIF5A bound 80S ribosome (**M**) Cryo-EM density of the eIF5A bound 80S ribosome colored according to local resolution. (**N**) Euler angle distribution of the final eIF5A bound 80S reconstruction. (**O)** Length distribution of mRNA fragments during selective ribosome profiling (monosome-enriched approach, fig. S5B) using Not4 as bait (bottom) and the total ribosomal fraction as control (top)..

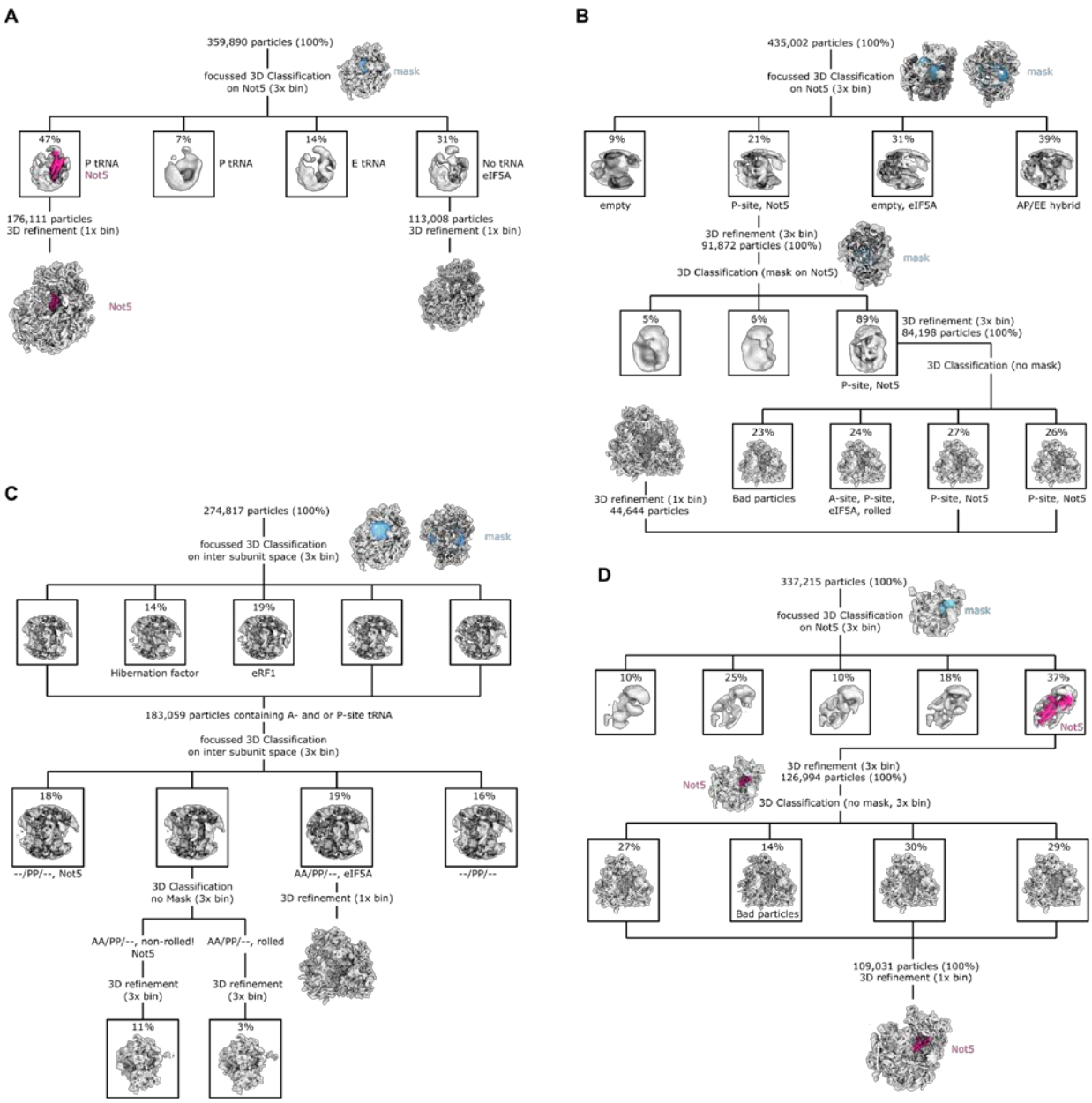

Fig. S4.

(**A**) Sorting scheme of the tigecycline stalled monosome sample. (**B**) Sorting scheme of the tigecycline stalled polysome sample. (**C**) Sorting scheme of the cycloheximide stalled monosome sample. (**D**) Sorting scheme of the tigecycline stalled cross-linked monosome sample.

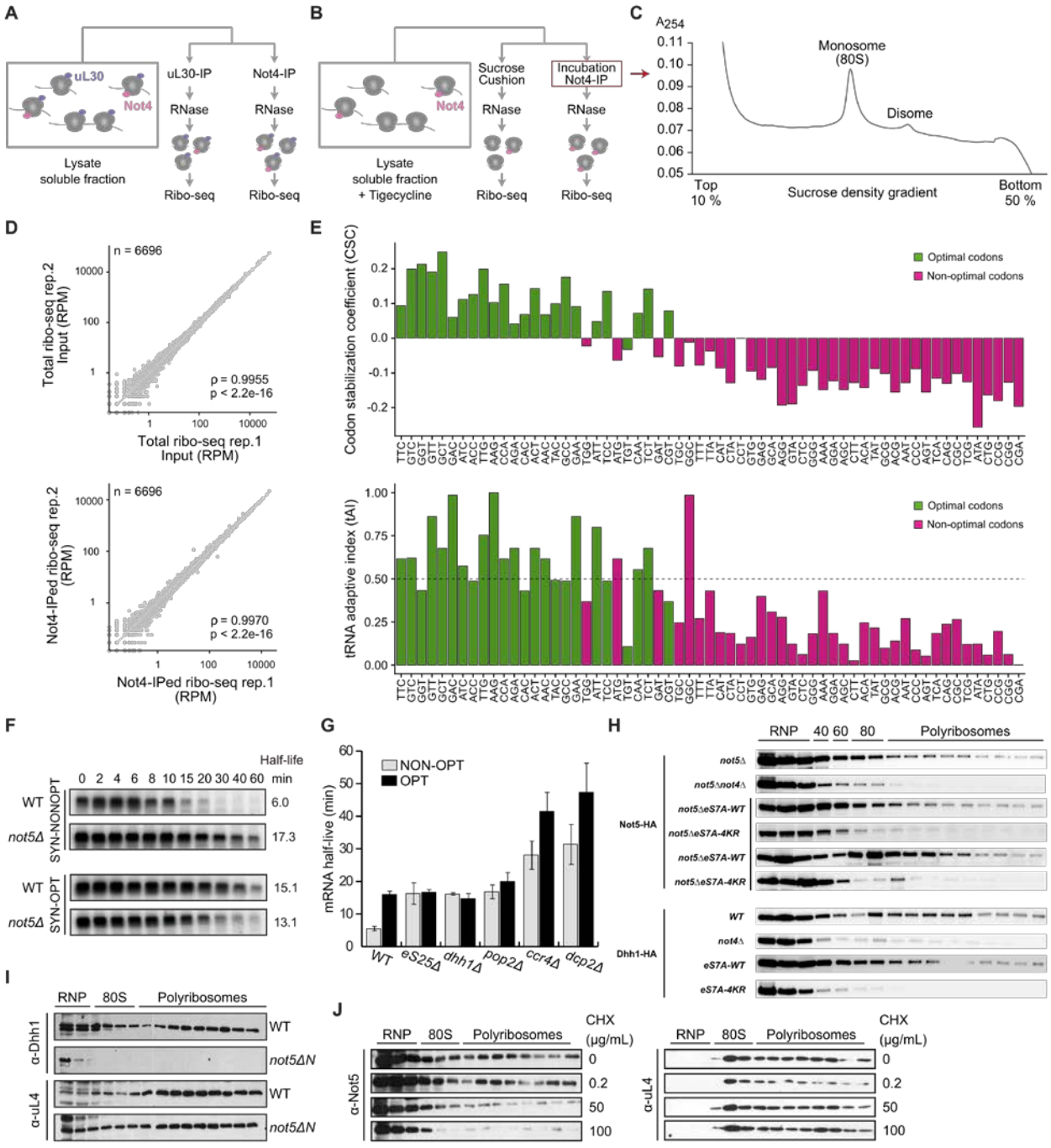

Fig. S5.

(**A**) Fast selective ribosome profiling approach. (**B** to **C**) Monosome-enriched selective ribosome profiling approach. (**D**) Quality control of the total ribosomal fraction (top) and the Not4-IP fraction (bottom) of the monosome-enriched selective ribosome profiling. (**E**) CSC of individual

codons present in the A-site listed according to their enrichment through Not4-IP (top). tAI of individual codons in the A-site listed according to their enrichment through Not4-IP (bottom). (**F**) Half-life determination of synthetic optimal and non-optimal *PGK1pG* reporter mRNAs through northern blotting at various timepoints after transcriptional shutoff (T) in either wildtype or *not5*Δ strains. (**G**) Half-lives of optimal and non-optimal PGK1pG reporter mRNAs in wildtype and *eS25*Δ, *dhh1*Δ, *pop2*Δ, *ccr4*Δ and *dcp2*Δ, as determined by northern blotting. (**H**) Top 6 lanes: Presence of Not5-HA on the translation machinery in *not5*Δ, *not5*Δ*not4*Δ, *eS7a-WT*, *eS7a-4KR* cells determined by Western blotting of sucrose density gradients. Bottom 4 lanes: Presence of Dhh1-HA on the translation machinery in *WT*, *not4*Δ, *eS7a-WT*, *eS7a-4KR* cells determined by Western blotting of sucrose density gradients. (**I**) Presence of Dhh1 (or uL4 as control) on the translation machinery determined by Western blotting of sucrose density gradients in wildtype and *not5*Δ*NTD* strains. (**J**) Presence of Not5 (or uL4 as control) on the translation machinery determined by Western blotting of sucrose density gradients in presence of different concentrations of cycloheximide.

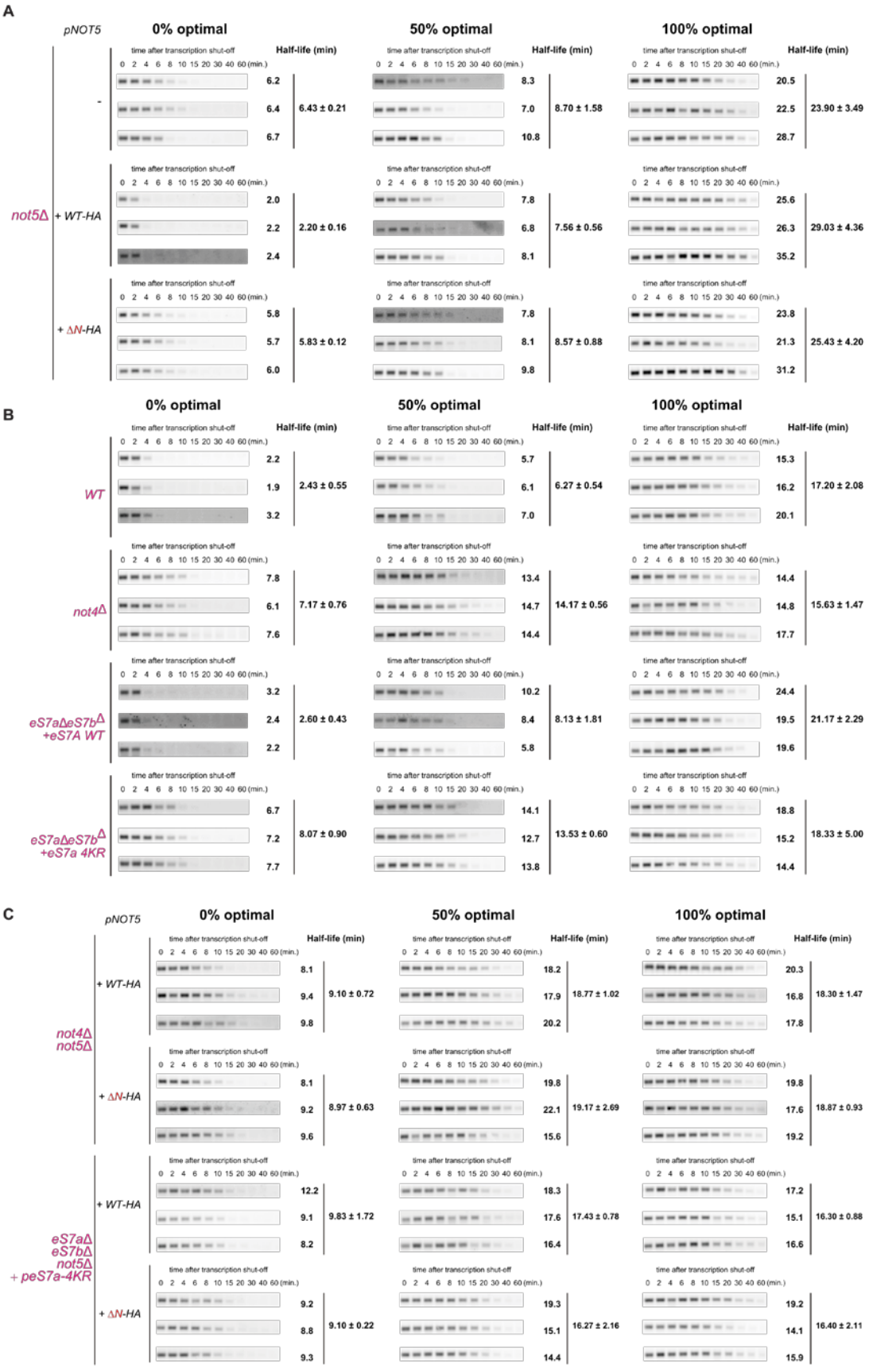
A
pNOT5
0% optimal
50% optimal
100% optimal
time after transcription shut-off
0 2 4 6 8 10 15 20 30 40 60 (min.)
Half-life (min)
-
6.2
6.4
6.7
6.43 ± 0.21
8.3
7.0
10.8
8.70 ± 1.58
20.5
22.5
28.7
23.90 ± 3.49
not5Δ + WT-HA
2.0
2.2
2.4
2.20 ± 0.16
7.8
6.8
8.1
7.56 ± 0.56
25.6
26.3
35.2
29.03 ± 4.36
+ ΔN-HA
5.8
5.7
6.0
5.83 ± 0.12
7.8
8.1
9.8
8.57 ± 0.88
23.8
21.3
31.2
25.43 ± 4.20
B
0% optimal
50% optimal
100% optimal
time after transcription shut-off
0 2 4 6 8 10 15 20 30 40 60 (min.)
Half-life (min)
WT
2.2
1.9
3.2
2.43 ± 0.55
5.7
6.1
7.0
6.27 ± 0.54
15.3
16.2
20.1
17.20 ± 2.08
not4Δ
7.8
6.1
7.6
7.17 ± 0.76
13.4
14.7
14.4
14.17 ± 0.56
14.4
14.8
17.7
15.63 ± 1.47
eS7aΔeS7bΔ +eS7A WT
3.2
2.4
2.2
2.60 ± 0.43
10.2
8.4
5.8
8.13 ± 1.81
24.4
19.5
19.6
21.17 ± 2.29
eS7aΔeS7bΔ +eS7a 4KR
6.7
7.2
7.7
8.07 ± 0.90
14.1
12.7
13.8
13.53 ± 0.60
18.8
15.2
14.4
18.33 ± 5.00
C
pNOT5
0% optimal
50% optimal
100% optimal
time after transcription shut-off
0 2 4 6 8 10 15 20 30 40 60 (min.)
Half-life (min)
not4Δ not5Δ
+ WT-HA
8.1
9.4
9.8
9.10 ± 0.72
18.2
17.9
20.2
18.77 ± 1.02
20.3
16.8
17.8
18.30 ± 1.47
+ ΔN-HA
8.1
9.2
9.6
8.97 ± 0.63
19.8
22.1
15.6
19.17 ± 2.69
19.8
17.6
19.2
18.87 ± 0.93
eS7aΔ eS7bΔ not5Δ + peS7a-4KR
+ WT-HA
12.2
9.1
8.2
9.83 ± 1.72
18.3
17.6
16.4
17.43 ± 0.78
17.2
15.1
16.6
16.30 ± 0.88
+ ΔN-HA
9.2
8.8
9.3
9.10 ± 0.22
19.3
15.1
14.4
16.27 ± 2.16
19.2
14.1
15.9
16.40 ± 2.11

Fig. S6.

(**A**) Northern blotting of *HIS3* reporter mRNA upon transcriptional shutoff in *not5*Δ cells in combination with expression of different constructs from plasmids (pNot5, pNot5-ΔN). (**B**) Northern blotting of *HIS3* reporter mRNA upon transcriptional shutoff in *WT*, *not4*Δ, *eS7a/b*Δ, *not5*Δ*eS7a/b*Δ cells in combination with expression of different constructs from plasmids (peS7a, peS7a-4KR). (**C**) Northern blotting of *HIS3* reporter mRNA upon transcriptional shutoff in *not4*Δ*not5*Δ cells in combination with expression of different constructs from plasmids (pNot5, pNot5-ΔN, peS7a, peS7a-4KR).

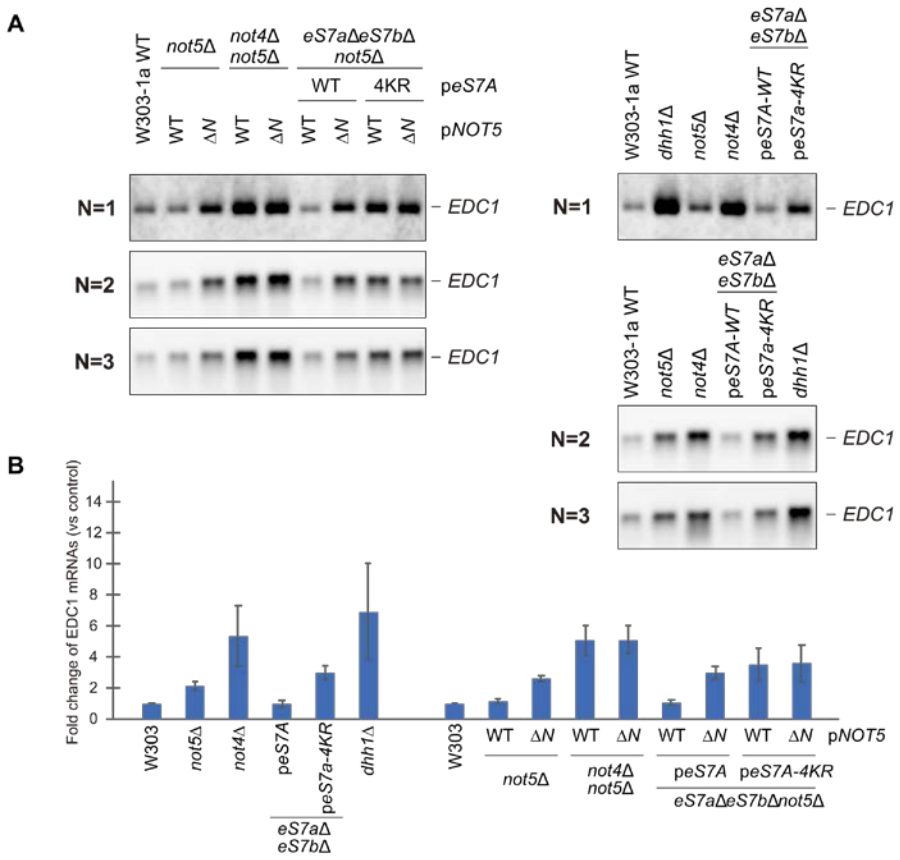

Fig. S7.

(**A**) Northern blots of EDC1 mRNA in different cell-lines. Stabilization of EDC1 mRNA, which is used as proxy for a decapping defect (**B**) Quantification of EDC1 mRNA stabilization based on the Northern Blots shown in (A) (data are mean +/- SD, N=3).

Table S1.

Cryo-EM data collection, refinement and validation statistics

	Not5-80S EMD-10431 PDB 6TB3	Not5-poly EMD-10431 -	eIF5A-80S EMD- 10537 PDB 6TNU	Not5-80S-xl EMD-10431 -
Data collection and processing				
Microscope	Titan Krios	Titan Krios	Titan Krios	Titan Krios
Detector	Falcon II	Falcon II	Falcon II	Falcon II
Automation software	EPU	EPU	EPU	EPU
Magnification	75,000	75,000	75,000	75,000
Voltage (kV)	300	300	300	300
Exposure rate (e^{-}/pix/s)	55	55	55	55
Electron exposure (e^{-}/Å^2)	28	28	28	28
Number of frames used	10	10	10	10
Defocus range (μm)	-1.1 – -2.8	-1.1 – -2.8	-1.1 – -2.8	-1.1 – -2.8
Pixel size (Å)	1.084	1.084	1.084	1.084
Symmetry imposed	-	-	-	-
Micrographs used	9,945	9,611	12,697	10,654
Initial particle images (no.)	557,059	828,516	1,378,230	589,191
Particle images used (no.)	359,890	435,002	274,817	337,215
Final particle images (no.)	176,111	44,644	50,989	109,031
Map overall resolution (Å)	2.8	3.2	3.1	2.9
FSC threshold	0.143	0.143	0.143	0.143
RS Refinement (Phenix)				
Initial model used (PDB code)	4V88	-	6TB3, 5GAK	-
Model resolution (Å)	2.6 / 2.8	-	2.9 / 3.1	-
FSC threshold	0.143 / 0.5	-	0.143 / 0.5	-
Map sharpening *B* factor (Å^2)	-80	-80	-80	-80
Model composition				
Nonhydrogen atoms	205,032	-	204,962	-
Protein residues	11,472	-	11,497	-
Nucleotides	5,351	-	5,391	
Ligands	335	-	10	-
mean *B* factors (Å^2)				
Protein	71.58	-	76.23	-
Ligand	40.82	-	47.83	-
R.m.s. deviations				
Bond lengths (Å)	0.006	-	0.009	-
Bond angles (°)	0.856	-	0.950	-
Validation				
MolProbity score	1.50	-	1.93	-
Clashscore	2.66	-	6.91	-
Poor rotamers (%)	0.27	-	0.01	-
Ramachandran plot				
Favored (%)	93.10	-	89.91	-
Outliers (%)	0.08	-	0.06	-
C-beta deviations (%)	0.01	-	0.00	-
CaBLAM outliers (%)	4.22		5.22	
Model-Map scores				
CC (mask/box/peaks/volume)	0.90/0.91/0.87/0.89	-	0.83/0.87/0.80/0.83	-
Mean CC for ligands	0.83	-	0.74	-
EMRinger score (Not5-NTD)	2.79	-	-	-

Table S2.

Yeast strains used in this study

Name	Genotype	Source
yJC151	MATa, ura3, leu2, his3, met15	(*46*)
yJC1708	ura3, leu2, his3, met15 or MET15, LYS2, not5::LEU2	This study
yJC1892	MATa, ura3, leu2, his3, met15 [pGAL-PGK1-SYNOP-pG, URA3]	(*4*)
yJC1893	MATa, ura3, leu2, his3, met15 [pGAL-PGK1-SYNNONOP-pG, URA3]	(*4*)
yJC1913	MATa, ura3, leu2, his3, met15, dhh1::NEO [pGAL-PGK1-SYNOP-pG, URA3]	(*4*)
yJC1914	MATa, ura3, leu2, his3, met15, dhh1::NEO [pGAL-PGK1-SYNNONOP-pG, URA3]	(*4*)
yJC1917	MATa, ura3, leu2, his3, lys2, dcp2::NEO [pGAL-PGK1-SYNOP-pG, URA3]	(*4*)
yJC1918	MATa, ura3, leu2, his3, lys2, dcp2::NEO [pGAL-PGK1-SYNNONOP-pG, URA3]	(*4*)
yJC1961	MATa, ura3, his3, leu2, met15, ccr4:NEO [pGAL-PGK1-SYNOP-pG, URA3]	(*4*)
yJC1962	MATa, ura3, leu2, his3, met15, ccr4::NEO [pGAL-PGK1-SYNNONOP-pG, URA3]	(*4*)
yJC2364	MATa, ura3, his3, leu2, met15, pop2::NEO [pGAL-PGK1-SYNOP-pG, URA3]	(*4*)
yJC2365	MATa, ura3, his3, leu2, met15, pop2::NEO [pGAL-PGK1-SYNNONOP-pG, URA3]	(*4*)
yJC2499	MATa, ura3, leu2, his3, met15, [N-terminally optimal FLAG tagged 0% optimal HIS3 under the control of the GAL1 promoter, URA3]	(*8*)
yJC2504	MATa, ura3, leu2, his3, met15, [N-terminally optimal FLAG tagged 50% optimal HIS3 under the control of the GAL1 promoter, URA3]	(*8*)
yJC2509	MATa, ura3, leu2, his3, met15, [N-terminally optimal FLAG tagged 100% optimal HIS3 under the control of the GAL1 promoter, URA3]	(*8*)
yJC2587	ura3, leu2, his3, met15 or MET15, LYS2, not5::LEU2, [pGAL-PGK1-SYNOP-pG, URA3]	This study

yJC2588	ura3, leu2, his3, met15 or MET15, LYS2, not5::LEU2, [pGAL-PGK1-SYNNONOP-pG, URA3]	This study
yJC2708	MATa, ura3, leu2, his3, met15, NOT5-HA::HIS	This study
yJC2721	ura3, leu2, his3, met15 or MET15, LYS2, not5::LEU2, [N-terminally optimal FLAG tagged 0% optimal HIS3 under the control of the GAL1 promoter, URA3]	This study
yJC2722	ura3, leu2, his3, met15 or MET15, LYS2, not5::LEU2, [N-terminally optimal FLAG tagged 50% optimal HIS3 under the control of the GAL1 promoter, URA3]	This study
yJC2723	ura3, leu2, his3, met15 or MET15, LYS2, not5::LEU2, [N-terminally optimal FLAG tagged 100% optimal HIS3 under the control of the GAL1 promoter, URA3]	This study
yJC2809	MATa, ura3, leu2, his3, lys2, rps25a::KANMX, rps25b::KANMX [pGAL-PGK1-SYNOP-pG, URA3]	This study
yJC2810	MATa, ura3, leu2, his3, lys2, rps25a::KANMX, rps25b::KANMX [pGAL-PGK1-SYNOP-pG, URA3]	This study
W303-1a	MATa ade2 his3 leu2 trp1 ura3 can1	Lab. Stock
Not4-FTPA	MATa ade2 his3 leu2 trp1 ura3 can1 NOT4-FTPA::natNT2	(*47*)
uL30-TAP	MATa ade2 his3 leu2 trp1 ura3 can1 uL30-TAP::TRP1	(*47*)
YLD258	MATa ade2 his3 leu2 trp1 ura3 can1 *not4*Δ::*kanMX6*	Lab. Stock
Y124	MATa ade2 his3 leu2 trp1 ura3 can1 *eS7a*Δ::*HIS3MX6 eS7b*Δ::*natNT2 p416-eS7A-HA*	Lab. Stock
YSG125	MATa ade2 his3 leu2 trp1 ura3 can1 *not5*Δ::*natNT2 p416-NOT5-HA*	This study
YSG131	MATa ade2 his3 leu2 trp1 ura3 can1 *not5*Δ::*HIS3MX6 not4*Δ::*kanMX6 p416NOT5-HA*	This study
YSG132	MATa ade2 his3 leu2 trp1 ura3 can1 *not5*Δ::*kanMX4 eS7a*Δ::*HIS3MX6 eS7b*Δ::*natNT2 p416-eS7A-HA*	This study
YSA024	MATa ade2 his3 leu2 trp1 ura3 can1 *dhh1*Δ::*kanMX4*	Lab. Stock

Table S3.
Plasmids and oligos used in this study

Name	Description	Source
pJC296	PGK1pG reporter (under control of GAL1 UAS)	(*46*)
pJC672	PGK1pG reporter with SYNOP ORF (under control of GAL1 UAS)	(*4*)
pJC673	PGK1pG reporter with SYNNONOP ORF (under control of GAL1 UAS)	(*4*)
pJC857	0% optimal HIS3 with N-terminal FLAG tag (GAL1 promoter)	(*8*)
pJC862	50% optimal HIS3 with N-terminal FLAG tag (GAL1 promoter)	(*8*)
pJC867	100% optimal HIS3 with N-terminal FLAG tag (GAL1 promoter)	(*8*)
pRS416-Not5-HA	CEN, URA3, Not5-HA (NOT5 promoter)	This study
pRS415	CEN, LEU2	Lab stock
pRS415-Not5-HA	CEN, LEU2, Not5-HA (NOT5 promoter)	This study
pRS415-Not5ΔNTD-HA	CEN, LEU2, Not5ΔNTD-HA (NOT5 promoter), the region from 2 to 113 A.A. is deleted	This study
pRS416-eS7-HA	CEN, URA3, eS7a-HA (eS7A promoter)	(*12*)
pRS315-eS7-HA	CEN, LEU2, eS7a-HA (eS7A promoter)	(*12*)
pRS315-eS7-4KR-HA	CEN, LEU2, eS7a-4KR-HA (eS7A promoter)	(*12*)
pYM032	CEN, ADE2, eS7a-WT-HA (eS7A promoter) in pASZ11	Lab stock
pYM033	CEN, ADE2, eS7a-4KR-HA (eS7A promoter) in pASZ11	Lab stock
pSM037	CEN, URA3, Dhh1-HA (GPD promoter)	Lab stock
Oligo oJC168	5’-AATTCCCCCCCCCCCCCCCCCCA-3’	(*46*)
Oligo oJC306	5’-GTCTAGCCGCGAGGAAGG-3’	(*46*)
Oligo oJC2564	5’-CCTGATCCAAACCTTTTTACTCC-3’	(*8*)

Movie S1.
Differential readout of slow translation elongation kinetics by eIF5A and Not5.

References and Notes

1. M. A. Collart, The Ccr4-Not complex is a key regulator of eukaryotic gene expression. *WIREs RNA* **7**, 438–454 (2016). doi:10.1002/wrna.1332 Medline

2. I. B. Schäfer, M. Yamashita, J. M. Schuller, S. Schüssler, P. Reichelt, M. Strauss, E. Conti, Molecular Basis for poly(A) RNP Architecture and Recognition by the Pan2-Pan3 Deadenylase. *Cell* **177**, 1619–1631.e21 (2019). doi:10.1016/j.cell.2019.04.013 Medline

3. R. Parker, RNA degradation in Saccharomyces cerevisae. *Genetics* **191**, 671–702 (2012). doi:10.1534/genetics.111.137265 Medline

4. V. Presnyak, N. Alhusaini, Y. H. Chen, S. Martin, N. Morris, N. Kline, S. Olson, D. Weinberg, K. E. Baker, B. R. Graveley, J. Coller, Codon optimality is a major determinant of mRNA stability. *Cell* **160**, 1111–1124 (2015). doi:10.1016/j.cell.2015.02.029 Medline

5. A. A. Bazzini, F. del Viso, M. A. Moreno-Mateos, T. G. Johnstone, C. E. Vejnar, Y. Qin, J. Yao, M. K. Khokha, A. J. Giraldez, Codon identity regulates mRNA stability and translation efficiency during the maternal-to-zygotic transition. *EMBO J.* **35**, 2087–2103 (2016). doi:10.15252/embj.201694699 Medline

6. Q. Wu, S. G. Medina, G. Kushawah, M. L. DeVore, L. A. Castellano, J. M. Hand, M. Wright, A. A. Bazzini, Translation affects mRNA stability in a codon-dependent manner in human cells. *eLife* **8**, e45396 (2019). doi:10.7554/eLife.45396 Medline

7. M. W. Webster, Y. H. Chen, J. A. W. Stowell, N. Alhusaini, T. Sweet, B. R. Graveley, J. Coller, L. A. Passmore, mRNA Deadenylation Is Coupled to Translation Rates by the Differential Activities of Ccr4-Not Nucleases. *Mol. Cell* **70**, 1089–1100.e8 (2018). doi:10.1016/j.molcel.2018.05.033 Medline

8. A. Radhakrishnan, Y. H. Chen, S. Martin, N. Alhusaini, R. Green, J. Coller, The DEAD-Box Protein Dhh1p Couples mRNA Decay and Translation by Monitoring Codon Optimality. *Cell* **167**, 122–132.e9 (2016). doi:10.1016/j.cell.2016.08.053 Medline

9. P. Tesina, E. Heckel, J. Cheng, M. Fromont-Racine, R. Buschauer, L. Kater, B. Beatrix, O. Berninghausen, A. Jacquier, T. Becker, R. Beckmann, Structure of the 80S ribosome-Xrn1 nuclease complex. *Nat. Struct. Mol. Biol.* **26**, 275–280 (2019). doi:10.1038/s41594-019-0202-5 Medline

10. L. N. Dimitrova, K. Kuroha, T. Tatematsu, T. Inada, Nascent peptide-dependent translation arrest leads to Not4p-mediated protein degradation by the proteasome. *J. Biol. Chem.* **284**, 10343–10352 (2009). doi:10.1074/jbc.M808840200 Medline

11. S. Preissler, J. Reuther, M. Koch, A. Scior, M. Bruderek, T. Frickey, E. Deuerling, Not4-dependent translational repression is important for cellular protein homeostasis in yeast. *EMBO J.* **34**, 1905–1924 (2015). doi:10.15252/embj.201490194 Medline

12. K. Ikeuchi, P. Tesina, Y. Matsuo, T. Sugiyama, J. Cheng, Y. Saeki, K. Tanaka, T. Becker, R. Beckmann, T. Inada, Collided ribosomes form a unique structural interface to induce Hel2-driven quality control pathways. *EMBO J.* **38**, e100276 (2019). doi:10.15252/embj.2018100276 Medline

13. O. O. Panasenko, M. A. Collart, Presence of Not5 and ubiquitinated Rps7A in polysome fractions depends upon the Not4 E3 ligase. *Mol. Microbiol.* **83**, 640–653 (2012). doi:10.1111/j.1365-2958.2011.07957.x Medline

14. Z. Villanyi, V. Ribaud, S. Kassem, O. O. Panasenko, Z. Pahi, I. Gupta, L. Steinmetz, I. Boros, M. A. Collart, The Not5 subunit of the ccr4-not complex connects transcription and translation. *PLOS Genet.* **10**, e1004569 (2014). doi:10.1371/journal.pgen.1004569 Medline

15. N. Alhusaini, J. Coller, The deadenylase components Not2p, Not3p, and Not5p promote mRNA decapping. *RNA* **22**, 709–721 (2016). doi:10.1261/rna.054742.115 Medline

16. D. Muhlrad, R. Parker, The yeast EDC1 mRNA undergoes deadenylation-independent decapping stimulated by Not2p, Not4p, and Not5p. *EMBO J.* **24**, 1033–1045 (2005). doi:10.1038/sj.emboj.7600560 Medline

17. R. Basavappa, P. B. Sigler, The 3 A crystal structure of yeast initiator tRNA: Functional implications in initiator/elongator discrimination. *EMBO J.* **10**, 3105–3111 (1991). doi:10.1002/j.1460-2075.1991.tb07864.x Medline

18. J. G. Tate, S. Bamford, H. C. Jubb, Z. Sondka, D. M. Beare, N. Bindal, H. Boutselakis, C. G. Cole, C. Creatore, E. Dawson, P. Fish, B. Harsha, C. Hathaway, S. C. Jupe, C. Y. Kok, K. Noble, L. Ponting, C. C. Ramshaw, C. E. Rye, H. E. Speedy, R. Stefancsik, S. L. Thompson, S. Wang, S. Ward, P. J. Campbell, S. A. Forbes, COSMIC: The Catalogue Of Somatic Mutations In Cancer. *Nucleic Acids Res.* **47**, D941–D947 (2019). doi:10.1093/nar/gky1015 Medline

19. K. De Keersmaecker, Z. K. Atak, N. Li, C. Vicente, S. Patchett, T. Girardi, V. Gianfelici, E. Geerdens, E. Clappier, M. Porcu, I. Lahortiga, R. Lucà, J. Yan, G. Hulselmans, H. Vranckx, R. Vandepoel, B. Sweron, K. Jacobs, N. Mentens, I. Wlodarska, B. Cauwelier, J. Cloos, J. Soulier, A. Uyttebroeck, C. Bagni, B. A. Hassan, P. Vandenberghe, A. W. Johnson, S. Aerts, J. Cools, Exome sequencing identifies mutation in CNOT3 and ribosomal genes RPL5 and RPL10 in T-cell acute lymphoblastic leukemia. *Nat. Genet.* **45**, 186–190 (2013). doi:10.1038/ng.2508 Medline

20. T. V. Budkevich, J. Giesebrecht, E. Behrmann, J. Loerke, D. J. Ramrath, T. Mielke, J. Ismer, P. W. Hildebrand, C. S. Tung, K. H. Nierhaus, K. Y. Sanbonmatsu, C. M. Spahn, Regulation of the mammalian elongation cycle by subunit rolling: A eukaryotic-specific ribosome rearrangement. *Cell* **158**, 121–131 (2014). doi:10.1016/j.cell.2014.04.044 Medline

21. C. Schmidt, T. Becker, A. Heuer, K. Braunger, V. Shanmuganathan, M. Pech, O. Berninghausen, D. N. Wilson, R. Beckmann, Structure of the hypusinylated eukaryotic translation factor eIF-5A bound to the ribosome. *Nucleic Acids Res.* **44**, 1944–1951 (2016). doi:10.1093/nar/gkv1517 Medline

22. C. C. Wu, B. Zinshteyn, K. A. Wehner, R. Green, High-Resolution Ribosome Profiling Defines Discrete Ribosome Elongation States and Translational Regulation during Cellular Stress. *Mol. Cell* **73**, 959–970.e5 (2019). doi:10.1016/j.molcel.2018.12.009 Medline

23. G. Hanson, N. Alhusaini, N. Morris, T. Sweet, J. Coller, Translation elongation and mRNA stability are coupled through the ribosomal A-site. *RNA* **24**, 1377–1389 (2018). doi:10.1261/rna.066787.118 Medline

24. A. D. Petropoulos, R. Green, Further in vitro exploration fails to support the allosteric three-site model. *J. Biol. Chem.* **287**, 11642–11648 (2012). doi:10.1074/jbc.C111.330068 Medline

25. T. Suzuki, C. Kikuguchi, S. Sharma, T. Sasaki, M. Tokumasu, S. Adachi, T. Natsume, Y. Kanegae, T. Yamamoto, CNOT3 suppression promotes necroptosis by stabilizing mRNAs for cell death-inducing proteins. *Sci. Rep.* **5**, 14779 (2015). doi:10.1038/srep14779 Medline

26. L. Y. Chan, C. F. Mugler, S. Heinrich, P. Vallotton, K. Weis, Non-invasive measurement of mRNA decay reveals translation initiation as the major determinant of mRNA stability. *eLife* **7**, e32536 (2018). doi:10.7554/eLife.32536 Medline

27. S. Sohrabi-Jahromi, K. B. Hofmann, A. Boltendahl, C. Roth, S. Gressel, C. Baejen, J. Soeding, P. Cramer, Transcriptome maps of general eukaryotic RNA degradation factors. *eLife* **8**, e47040 (2019). doi:10.7554/eLife.47040 Medline

28. O. O. Panasenko, S. P. Somasekharan, Z. Villanyi, M. Zagatti, F. Bezrukov, R. Rashpa, J. Cornut, J. Iqbal, M. Longis, S. H. Carl, C. Peña, V. G. Panse, M. A. Collart, Co-translational assembly of proteasome subunits in NOT1-containing assemblysomes. *Nat. Struct. Mol. Biol.* **26**, 110–120 (2019). doi:10.1038/s41594-018-0179-5 Medline

29. M. S. Longtine, A. McKenzie 3rd, D. J. Demarini, N. G. Shah, A. Wach, A. Brachat, P. Philippsen, J. R. Pringle, Additional modules for versatile and economical PCR-based gene deletion and modification in Saccharomyces cerevisiae. *Yeast* **14**, 953–961 (1998). doi:10.1002/(SICI)1097-0061(199807)14:10<953:AID-YEA293>3.0.CO;2-U Medline

30. C. Janke, M. M. Magiera, N. Rathfelder, C. Taxis, S. Reber, H. Maekawa, A. Moreno-Borchart, G. Doenges, E. Schwob, E. Schiebel, M. Knop, A versatile toolbox for PCR-based tagging of yeast genes: New fluorescent proteins, more markers and promoter substitution cassettes. *Yeast* **21**, 947–962 (2004). doi:10.1002/yea.1142 Medline

31. S. Q. Zheng, E. Palovcak, J. P. Armache, K. A. Verba, Y. Cheng, D. A. Agard, MotionCor2: Anisotropic correction of beam-induced motion for improved cryo-electron microscopy. *Nat. Methods* **14**, 331–332 (2017). doi:10.1038/nmeth.4193 Medline

32. K. Zhang, Gctf: Real-time CTF determination and correction. *J. Struct. Biol.* **193**, 1–12 (2016). doi:10.1016/j.jsb.2015.11.003 Medline

33. D. Kimanius, B. O. Forsberg, S. H. Scheres, E. Lindahl, Accelerated cryo-EM structure determination with parallelisation using GPUs in RELION-2. *eLife* **5**, e18722 (2016). doi:10.7554/eLife.18722 Medline

34. J. Zivanov, T. Nakane, B. O. Forsberg, D. Kimanius, W. J. Hagen, E. Lindahl, S. H. Scheres, New tools for automated high-resolution cryo-EM structure determination in RELION-3. *eLife* **7**, e42166 (2018). doi:10.7554/eLife.42166 Medline

35. P. Emsley, K. Cowtan, Coot: Model-building tools for molecular graphics. *Acta Crystallogr. D* **60**, 2126–2132 (2004). doi:10.1107/S0907444904019158 Medline

36. P. V. Afonine, R. W. Grosse-Kunstleve, N. Echols, J. J. Headd, N. W. Moriarty, M. Mustyakimov, T. C. Terwilliger, A. Urzhumtsev, P. H. Zwart, P. D. Adams, Towards automated crystallographic structure refinement with phenix.refine. *Acta Crystallogr. D* **68**, 352–367 (2012). doi:10.1107/S0907444912001308 Medline

37. T. D. Goddard, C. C. Huang, E. C. Meng, E. F. Pettersen, G. S. Couch, J. H. Morris, T. E. Ferrin, UCSF ChimeraX: Meeting modern challenges in visualization and analysis. *Protein Sci.* **27**, 14–25 (2018). doi:10.1002/pro.3235 Medline

38. N. T. Ingolia, G. A. Brar, S. Rouskin, A. M. McGeachy, J. S. Weissman, The ribosome profiling strategy for monitoring translation in vivo by deep sequencing of ribosome-protected mRNA fragments. *Nat. Protoc.* **7**, 1534–1550 (2012). doi:10.1038/nprot.2012.086 Medline

39. T. Smith, A. Heger, I. Sudbery, UMI-tools: Modeling sequencing errors in Unique Molecular Identifiers to improve quantification accuracy. *Genome Res.* **27**, 491–499 (2017). doi:10.1101/gr.209601.116 Medline

40. J. G. Dunn, J. S. Weissman, Plastid: Nucleotide-resolution analysis of next-generation sequencing and genomics data. *BMC Genomics* **17**, 958 (2016). doi:10.1186/s12864-016-3278-x Medline

41. C. J. Woolstenhulme, N. R. Guydosh, R. Green, A. R. Buskirk, High-precision analysis of translational pausing by ribosome profiling in bacteria lacking EFP. *Cell Rep.* **11**, 13–21 (2015). doi:10.1016/j.celrep.2015.03.014 Medline

42. S. Anders, W. Huber, Differential expression analysis for sequence count data. *Genome Biol.* **11**, R106 (2010). doi:10.1186/gb-2010-11-10-r106 Medline

43. S. Pechmann, J. Frydman, Evolutionary conservation of codon optimality reveals hidden signatures of cotranslational folding. *Nat. Struct. Mol. Biol.* **20**, 237–243 (2013). doi:10.1038/nsmb.2466 Medline

44. D. A. Drummond, A. Raval, C. O. Wilke, A single determinant dominates the rate of yeast protein evolution. *Mol. Biol. Evol.* **23**, 327–337 (2006). doi:10.1093/molbev/msj038 Medline

45. T. Sweet, C. Kovalak, J. Coller, The DEAD-box protein Dhh1 promotes decapping by slowing ribosome movement. *PLOS Biol.* **10**, e1001342 (2012). doi:10.1371/journal.pbio.1001342 Medline

46. W. Hu, T. J. Sweet, S. Chamnongpol, K. E. Baker, J. Coller, Co-translational mRNA decay in Saccharomyces cerevisiae. *Nature* **461**, 225–229 (2009). doi:10.1038/nature08265 Medline

47. Y. Matsuo, K. Ikeuchi, Y. Saeki, S. Iwasaki, C. Schmidt, T. Udagawa, F. Sato, H. Tsuchiya, T. Becker, K. Tanaka, N. T. Ingolia, R. Beckmann, T. Inada, Ubiquitination of stalled ribosome triggers ribosome-associated quality control. *Nat. Commun.* **8**, 159 (2017). doi:10.1038/s41467-017-00188-1 Medline